Characterization of flexural acoustic waves in optical fibers using a fiber-tip interferometer

Bello-Jiménez Miguel[1], Hernández-Escobar Erika[1], Navarro-Martínez Yareli[1*], López-Estopier Rosa[1,2], Hernández-Arriaga Marco[1], Pottiez Oliver[3], Durán-Sánchez Manuel[4], Ibarra-Escamilla Baldemar[4] and Andrés Miguel[5]

[1] Instituto de Investigación en Comunicación Óptica, Universidad Autónoma de San Luis Potosí, Av. Karakorum 1470 Lomas 4ª Secc., 78210, San Luis Potosí, México
[2] Consejo Nacional de Humanidades, Ciencia y Tecnología (CONAHCyT), Av. Insurgentes Sur 1582, Col. Crédito Constructor, Del. Benito Juárez, México, 039040, Ciudad de México
[3] Centro de Investigaciones en Óptica, A.C. (CIO), Loma del Bosque 115, Col. Lomas del Campestre, 37150 León, Guanajuato, México
[4] Instituto Nacional de Astrofísica, Óptica y Electrónica (INAOE), Luis Enrique Erro, Departamento de Óptica, 72000 Puebla, México
[5] Universidad de Valencia, Departamento de Física Aplicada y Electromagnetismo, ICMUV, c/Dr. Moliner 50, Burjassot, 46100 Valencia, Spain

E-mail: *a268990@alumnos.uaslp.mx

Abstract

An experimental study using a fiber tip interferometer (FTI) to characterize traveling flexural acoustic waves (TFAWs) along an optical fiber is reported. The measurements carried out with the FTI are performed following two different procedures: one of them relies on adjusting the interferometer at the quadrature condition and the other extracts the information from the amplitudes of the fundamental and second harmonic of the interference signal. From our measurements, the detection limit of the FTI is 0.5 nm and the upper limit of the linear regime is 30 nm. These results validate the use of the FTI to detect nanometric displacements associated to the amplitude of acoustic waves along an optical fiber. Parameters such as the acoustic wavelength, attenuation coefficient, and phase velocity are measured for a range of acoustic frequencies around the 2-MHz region. Furthermore, and supported by the in-fiber acousto-optic (AO) effect produced by TFAWs, parameters associated to an acoustic wave packet such as the group velocity and the group attenuation coefficient are also determined. This set of experimental results provide useful information of the mechanisms underlying the propagation of TFAWs along an optical fiber and its corresponding AO effect.

Keywords: Fiber-based interferometer sensors, All-fiber acousto-optic devices, In-fiber acousto-optic effect

---

1. Introduction

Fiber-based interferometers with characteristics of high accuracy, low cost, and easy implementation, are very attractive photonic devices with a great variety of application in diverse fields of science and industry. Examples of these applications include the measurement of different physical magnitudes, such as pressure [1-3], temperature [4-7], strain [8-10], refractive index [11-13], among others [14-16]. All these approaches offer the advantages of high resolution, easy alignment, simplicity in fabrication, and long-term stability. The operation principle of a fiber-based interferometer usually relies on the interference between two propagating light beams, denoted as the reference and measurement beams, which travel through different optical path lengths to subsequently meet and interfere. Hence, the resulting interference signal determines, as a function of the amount of change in the intensity, frequency, wavelength or phase, the sensing properties for the fiber interferometer. Nevertheless, and despite the abundant scientific publications related to fiber-based interferometer systems to detect nanometer-scale vibration amplitudes [17-24], the optimal conditions and operation limits for measuring nanometric displacements is usually not discussed in the reported publications. For this reason, this work focuses on determining the operational conditions of a fiber-tip interferometer (FTI) sensor to characterize the parameters associated to traveling flexural acoustic waves (TFAWs), such as the acoustic wave amplitude, phase velocity, acoustic wavelength, and the attenuation coefficient. In addition, taking advantage of the in-fiber acousto-optic (AO) effect generated by TFAWs, parameters related to an acoustic wave packet such as the group velocity or the group attenuation coefficient are also reported.

In recent years, in-fiber AO devices based on TFAWs have been proposed for the development of advanced all-fiber devices, such as AO mode converters [25-27], tunable band-pass filters [28-31] and active modulators within fiber laser systems [32-35], as well as for the development of accurate fiber characterization techniques [36,37]. In those approaches, a flexural acoustic wave is excited through a metal or silica horn, which is attached to a piezoelectric ceramic element to concentrate the acoustic vibrations into the optical fiber. In consequence, when a flexural acoustic wave is generated, it propagates along the optical fiber producing a periodic perturbation of the fiber refractive index that can lead to an intermodal resonant coupling between the fundamental core mode and some specific asymmetric cladding modes of the optical fiber [38,39]. The efficiency of the intermodal coupling depends on the amplitude and frequency of the acoustic flexural wave along the fiber. Therefore, to obtain a deeper insight into the in-fiber AO effect based on flexural waves, it is worth analyzing a method to characterize the properties of TFAWs along a standard optical fiber, which is the purpose of this work. For this aim to be achieved, the range of the acoustic wave frequencies is delimited to be around 2 MHz, in order to produce an in-fiber AO effect within the 1550-nm optical wavelength region, which is the optimal operation band for the transmission of light signals in a standard optical fiber.

In this paper, an experimental study for measuring nanometer-scale displacements by using an extrinsic FTI is reported. The interferometer consists of a compact and simple structure, in which a cleaved optical fiber tip is used as the sensing arm to detect small amplitude displacements associated to TFAWs. The measurements have been carried out following two different methods: one of them relies on adjusting the interferometer at quadrature, and the other is based on measuring the amplitudes of the fundamental and second harmonic of the interference signal. From our experimental results, a range of operation from 0.5 nm to 30 nm is obtained, demonstrating the potential use of the FTI to characterize the amplitude of flexural acoustic waves along a standard optical fiber. The parameters of the acoustic wave are reported for a range of acoustic frequencies in the 2-MHz region, in terms of the acoustic wave amplitude, acoustic power, attenuation coefficient, phase velocity, and the acoustic wavelength. In addition, the AO effect produced by TFAWs is also implemented to achieve a more complete characterization of the acoustic wave. In this manner, the intermodal coupling effect in the 1550-nm spectral region is generated for a standard optical fiber when an acoustic wave packet is traveling along the fiber, allowing to evaluate parameters such as the group velocity and the group attenuation coefficient. In this last set of measurements, the acoustic frequency was varied in a range between 2.4 MHz and 2.7 MHz, because frequencies in that range yield a maximal optical resonant condition from 1570 nm to 1520 nm, respectively, falling within the available spectral range of our tunable laser source. The presented results, to the best of our knowledge, could be considered one of the first works reporting a complete characterization for TFAWs within the range of 2-MHz acoustic frequencies and intermodal AO effect around the 1550-nm spectral region. These results provide important findings associated to the nature of the in-fiber AO effect and the TFAWs along a standard optical fiber.

2. Interferometer configuration and measurement principle

A schematic view of the experimental setup is illustrated in Figure 1. It is based on an extrinsic FTI, whose operation relies on Fresnel reflection at the tip of the sensing arm [40]. In this way, by cleaving its end face with a zero-degree angle, from the amount of light transmitted through the sensing arm, a portion of around 4% is returned back due at the core-air interface, denoted as the reference signal (I_R), meanwhile the

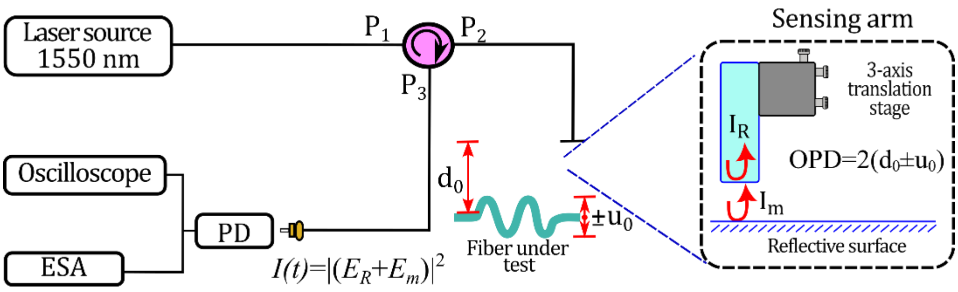

Figure 1. Experimental setup of the fiber-tip interferometer sensor. The expression $I(t)=|(E_R+E_m)|^2$ represents the interference signal resulting from the fields corresponding to the reference (E_R) and measurement (E_m) beams. The optical path difference (OPD) is given by $OPD=2(d_0\pm u_0)$.

rest of the transmitted light, denoted as the measurement signal (I_m), reaches the fiber under test (FUT), and it returns back to the interferometer due to Fresnel reflection at the air-fiber interface, thus yielding a longer optical path length for the measurement beam that depends on the separation distance, [d_0–u_0, d_0+u_0], between the sensing arm and the FUT. Thus, both reflected beams pass through port P_3 of the circulator and interfere, generating an interference signal ($I(t)$) that depends on the phase difference between the reference and measurement signals. The FTI consists of a three-port fiber-optic circulator, so that the light can be transmitted from port one (P_1) to the sensing arm of the interferometer via port two (P_2) of the circulator. A pigtailed tunable laser diode (TLD) source, delivering a maximum output power of 12 mW with a tunable spectral range from 1520 nm to 1570 nm (New Focus TLB-6728-P) is connected to port P_1 to perform the interferometric measurements. For this aim, the TLD is operated at 1550 nm. Measurements of the interference pattern were performed with a 17-MHz photodetector (PD, Thorlabs PDA10CS), a 2.5-GHz oscilloscope (Agilent Technologies DSO-X 6004 A) and a 3.2-GHz electrical spectrum analyzer (ESA, Siglent SSA 3032X). As illustrated in Figure1, the sensing arm of the FTI is mounted on a 3-axis linear translation stage with 26-nm resolution (Thorlabs NanoMax 300) to achieve fine adjustment of the separation distance d_0 and the measurement of the flexural acoustic wave amplitude (u_0). In the following subsections, the performance of the FTI to detect nanometer-scale displacements due TFAWs is reported following two different measurement methods. One of them bases its operation principle on adjusting the FTI at the quadrature condition [41-44], whereas the other method relies on measuring the harmonics of the interference signal [45-48] to extract information of the displacement amplitude.

2.1 The condition of quadrature and nanometer-scale displacement detection

The interference signal $I(t)$ is measured at the output port P_3 of the fiber circulator. Neglecting multi-reflections on the fiber tip and the FUT, the interferometric signal is obtained by superposition of the reference (E_R) and measurement (E_m) optical fields as

$$I(t) = I_0\left[1 + V\cos\left(\frac{4\pi\, u(t)}{\lambda_0} + \varphi_0\right)\right], \quad (1)$$

where k is the wave number ($k = 2\pi/\lambda_0$, being λ_0 the optical wavelength), $u(t)$ is the FUT displacement with respect the rest position ($u(t) = u_0 \sin(\Omega t)$, being u_0 the amplitude and Ω the

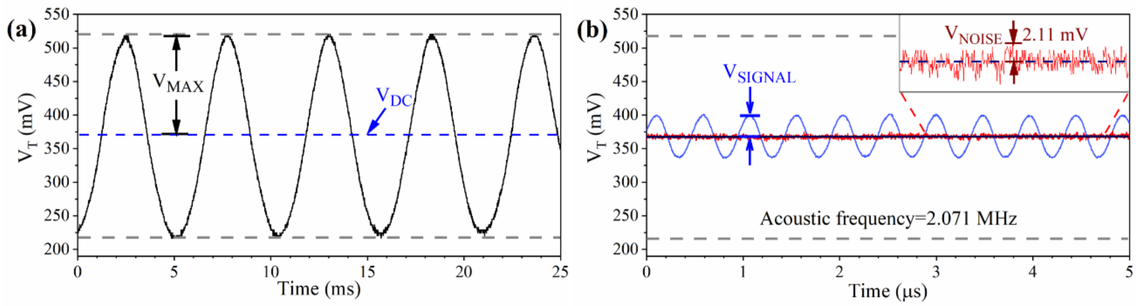

Figure 2. Oscilloscope traces corresponding to (a) real-time measurement of the interference signal when of φ_0 changes linearly with time, and (b) interference signal of the FTI in quadrature when a flexural wave propagates along the fiber. The red line is V_{DC}, and the blue line is the trace produced by the propagation of a flexural acoustic wave (a peak-to-peak voltage of 31 V and 2.071 MHz were used to drive the PZT disk). The inset illustrates the noise amplitude of the interferometric system.

angular frequency of the acoustic wave), φ_0 is the initial phase difference, which is directly related to the distance d_0 (the thickness of the formed extrinsic Fabry-Perot cavity), I_0 represents the sum of the reference (I_R) and measurement (I_m) intensities coupled back in the fiber, and V is the fringe visibility. Real-time measurements of the interference signal are presented in Figure 2. The interference trace is recorded in the oscilloscope by turning the light intensity into a voltage signal $V(t)$ through the responsivity of the photodetector and the impedance of the oscilloscope. Hence, the expression that describes the measured oscilloscope trace has the form

$$V(t) = V_{DC} + V_{MAX}\, cos\left(\frac{4\pi\, u(t)}{\lambda_0} + \varphi_0\right), \quad (2)$$

where $V(t)$ is a voltage proportional to the intensity signal, V_{DC} is a constant level of voltage and V_{MAX} is the amplitude related to the interference term. Figure 2(a) depicts a few interferometric fringes produced by a linear displacement applied to the sensing arm of the interferometer, that modulates φ_0 linearly with time, showing $V(t)$, V_{DC} and V_{MAX} voltages when 12 mW of input power is launched into port P_1. Therefore, to detect small oscillating amplitudes, the optimum operation point of the FTI is set at the maximal slope of the interference curve, where the maximum sensitivity and linearity are obtained. Consequently, to achieve nanometer-scale resolution, the interferometer is required to be operated under the quadrature condition, when the initial phase difference between interfering beams (φ_0) is an odd integer multiple of $\pi/2$. Thus, by carefully adjusting the position of the sensing arm via the 3-axis linear translation stage, the interferometer is positioned in quadrature. Figure 2(b) illustrates the oscilloscope trace by operating the interferometer in quadrature. The red line is V_{DC}, whereas the blue line is the oscillating time signal produced by the propagation of a flexural acoustic wave along the fiber. The V_{SIGNAL} voltage is the amplitude of the oscillating trace obtained when the interferometer is in quadrature, and the V_{NOISE} voltage, measured as the root-mean-square (RMS) value of V_{DC} when no flexural wave propagates, determines the detection limit of the interferometer ($3 \times V_{NOISE}$) [49].

The measured intensity signal within the quadrature condition, by considering an initial phase difference between beams (φ_0) equal to $\pi/2$, is expressed by

$$V_{SIGNAL} = V_{MAX}\, \sin\left(\frac{4\pi u_0}{\lambda_0}\right). \quad (3)$$

Assuming that the flexural wave will have always a small amplitude, that is $4\pi u_0/\lambda_0 \ll 1$, the displacement amplitude (u_0) can be calculated by using the small-angle (θ) approximation, namely $sin\ \theta \approx \theta$, from which the following equation is obtained

$$u_0 = \frac{\lambda_0}{4\pi}\left(\frac{V_{SIGNAL}}{V_{MAX}}\right). \quad (4)$$

In this way, the detection limit of the interferometer can be calculated by considering the criterium of 3 times the RMS value of the noise amplitude. Since V_{NOISE} measures 2.11 mV as presented in Figure 2(b), the calculated detection limit is 5.1 nm. This detection limit represents a condition where no special treatment is applied to noise amplitude, therefore, there exist a high potential for improvement if the noise amplitude is reduced. Conversely, an estimation of the maximum displacement is estimated from the maximum value that fulfills the small angle condition in equation (3), this value is estimated to be around 0.2441 radians for a relative error <1%. In such a case, the upper limit for the linear response regimen is 30.1 nm. Hence, the detection limits of the FTI system ranges from 5.1 nm to 30.1 nm. However, it is worth mentioning that this measurement range can be significantly improved by averaging the detected interference signal to reduce the noise contribution. For the measurements presented in this work, when the oscilloscope trace is averaged 4 times, we obtain an improved detection limit of 0.5 nm. For the values shown in Figure 2, V_{MAX} equal to 151.9 mV and V_{SIGNAL} equal to 32.62 mV, an amplitude measurement of 26.5 nm is obtained for the TFAW.

2.2 Amplitude detection by the harmonics of the interference signal

An alternative method to evaluate the oscillating displacement produced by a TFAW along the standard optical fiber relies on measuring the amplitude of the fundamental and second harmonic of the interference signal. In this way, the displacement produced by the acoustic wave can be expressed in the following form

$$d = d_0 + u_0 \sin(\Omega t), \quad (5)$$

where u_0 represents the acoustic wave amplitude, d_0 is the initial separation between the tip of the sensing arm and the oscillating surface, Ω is the oscillating angular frequency and t represents the time. By substituting this expression into equation (1), and using the Jacobi-Anger identity [49] to expand the interference signal into harmonic amplitudes, the measured intensity signal at the oscilloscope can be written as [50]

$$\begin{aligned} V(t) \propto\ & \cos(2kd_0 + \phi)[J_0(2ku_0) \\ & +2J_2(2ku_0)\cos(2\Omega t) + \cdots] \\ & -\sin(2kd_0 + \phi)[2J_1(2ku_0)\sin(\Omega t) \\ & +2J_3(2ku_0)\sin(3\Omega t) + \cdots] \end{aligned} \quad (6)$$

where $J_n(x)$ correspond to the Bessel function of first kind of order n, k indicates the wave number and ϕ represents a parameter that considers the slow amplitude fluctuations due to external perturbations, for example, variations of environmental conditions or low frequency mechanical vibrations of the interferometric system. Equation (6) is proportional to the harmonics that compose the detected signal, which in turns depend on the vibration amplitude u_0. To quantify the amplitude of a flexural acoustic wave, the vibration amplitude is related to the magnitude of the harmonics. For this purpose, an electrical spectrum analyzer (ESA) is employed to analyze the detected signal in terms of the harmonic amplitudes. An example of this measurement is illustrated in Figure 3, where a RF spectrum of the detected signal is measured within a 10-MHz span with 3-kHz resolution bandwidth.

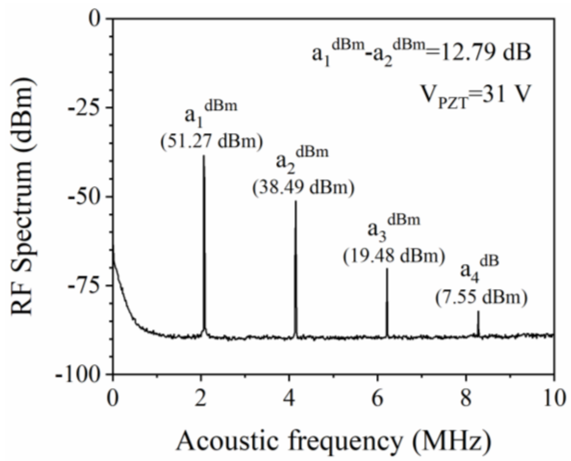

Figure 3. Measured RF spectrum for a 2.071 MHz traveling flexural acoustic wave. The RF voltage, corresponding to a peak-to-peak value of 31 V was used to drive the PZT disk (V_{PZT}).

The spectrum is obtained by averaging during a long enough time to measure the terms $\cos(2kd_0+\phi)$ and $\sin(2kd_0+\phi)$ in equation (6). Under this condition, the averaged amplitude of the fundamental frequency (a_1^{dBm}) and the second harmonic (a_2^{dBm}), both measured in decibels, are utilized to estimate the vibration amplitude via the ratio of their amplitudes, as is shown in the following equation

$$10^{(a_1^{dBm}-a_2^{dBm})/10} = \frac{J_1(2ku_0)}{J_2(2ku_0)}. \qquad (7)$$

By substituting the amplitude difference of 12.79 dB into equation (7) and solving numerically, an acoustic amplitude u_0 equal to 25.9 nm is obtained from the 64 averaged spectrums. For this method, a detection limit of around four nanometers is achieved. This detection limit strongly depends on the minimum detectable amplitude of the second harmonic. For our measurement system, it was detected with a minimal amplitude of 6.28 dB above the noise level background. Assuming the criterium of 3 times the RMS value for the noise amplitude, V_{NOISE} = 1.7 mV for the presented case, the detection limit for this technique is calculated as 4.1 nm. In the following section, a characterization of traveling flexural acoustic waves along a standard optical fiber is performed considering the two described measurement methods.

3. Experimental results and discussion

The experimental setup to generate a flexural acoustic wave along an optical fiber is depicted in Figure 4. It consists of a radiofrequency (RF) source used to drive a 20-mm diameter piezoelectric disk (PZT, Morgan Electroceramics based on PZT-5H piezoceramic material), which operates in the frequency region of 2-MHz and possesses 1-nm thickness. An aluminum concentrator horn is attached to the PZT and focuses the acoustic vibrations into the standard optica
l fiber (SMF-28) through its tip. The fiber is stripped from its outer polymer jacket to allow simultaneously the propagation of the acoustic wave and the intermodal coupling effect, the total length of the uncoated section of the optical fiber determines the AO interaction length (L). It is adjusted in a range between 4 cm and 1 m for the set of experiments

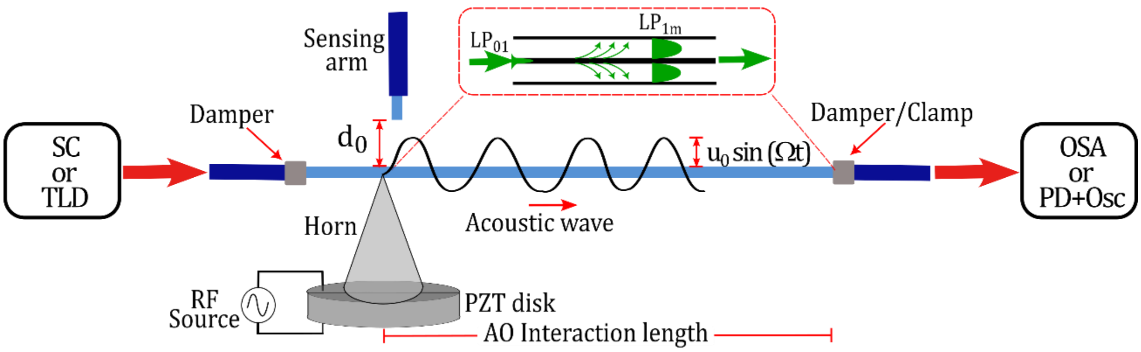

Figure 4. Experimental setup showing the generation and detection of a TFAW along a standard optical fiber. The inset illustrates the intermodal coupling between the core and cladding modes in an optical fiber.

reported here, with an interaction length that depends on the acoustic parameter to characterize. Additionally, acoustic dampers are located at both ends of the uncoated optical fiber, thus avoiding unwanted acoustic reflections. Notwithstanding, for measurements requiring of acoustic reflection, the end of the fiber opposite to the aluminum horn is firmly clamped to induce acoustic reflection and generate a standing flexural acoustic wave. Furthermore, since the acoustic wave amplitude is estimated to be on the order of a few tens of nanometers, initial measurements on the acoustic wave amplitude were performed under the quadrature condition, where a maximum sensitivity and linear response of the interferometer is anticipated. When analyzing a comparison of the intermodal coupling of light for different wavelengths, a supercontinuum source (SC) is employed at the system's input, while the output is connected to an optical spectrum analyzer (OSA, Anritsu MS9740A). However, for certain measurements, it is necessary to observe the coupling behavior for a specific wavelength. In such cases, the previously mentioned TLD is placed at the input, and at the output, it is connected to a PD (Newport 2011), which is subsequently connected to the oscilloscope to analyze the signal.

The in-fiber acousto-optic effect based on flexural acoustic waves depends on the periodic microbendings that results from the TFAW along the fiber. With a proper selection of the acoustic wave parameters, such as amplitude and frequency, this AO interaction can be implemented to the design of novel types of in-fiber AO devices, whose operation principle relies on the intermodal coupling between the fundamental core mode (LP_{01}) and some specific cladding modes (LP_{1m}) of the fiber. Therefore, it is worth analyzing in more detail the properties of flexural acoustic wave to obtain a greater insight into the in-fiber AO effect.

3.1 Frequency response and acoustic wave amplitude

A common feature of the PZT actuator is a non-flat frequency response, and its origin could be attributed to several factors, for example, the specific geometry of the piezoelectric disc and the resonant frequencies of the mounting structure, thus imposing restrictions and limitations on the operational PZT frequencies. To illustrate this behavior, the RF spectrum is measured for the oscillating interference signal that results from the propagation of a TFAW along the fiber. For this experiment, the applied voltage to the PZT disk (V_{PZT}) was maintained fixed at 32 V (whenever we refer to this voltage, it is a peak-to-peak measurement) through the experimental process, whereas the frequency is varied in a range from 1.06 to 3.17 MHz in a scheme that consists of a 23-cm interaction length. Figure 5(a) displays the measured RF spectra (fundamental harmonic) to expose the non-flat frequency response of the PZT disk. From this result, the best performance of the PZT element corresponds to the highest peak located at 2.071 MHz. At this frequency, LP_{01}−LP_{11} intermodal coupling is generated at the resonant optical wavelength of 1583.64 nm, as it is shown in Figure 5(b).

The amplitude u_0 of the flexural acoustic wave is measured considering the two methods described in section 2. With the first method, u_0 is measured as 26.5 nm, whereas the amplitude measurement by the harmonic frequencies reveals an acoustic amplitude of 25.9 nm. These two results could be considered in good agreement, since the difference between the measured amplitudes (0.6 nm) is very close to the detection limit of the FTI (0.5 nm). With the objective of analyzing the variations in amplitude for the acoustic wave as a function of the applied V_{PZT}, the latter is varied from 5 V to 33 V. This voltage range was selected to ensure a stable and linear response of the PZT, plus avoiding a degradation of the PZT response due to an excessive heating. Figure 6(a) illustrates the measured acoustic wave amplitudes considering both measurement methods. As it can be observed, both measurements are nearly equivalent, displaying a percent error with respect to the measurements based on the

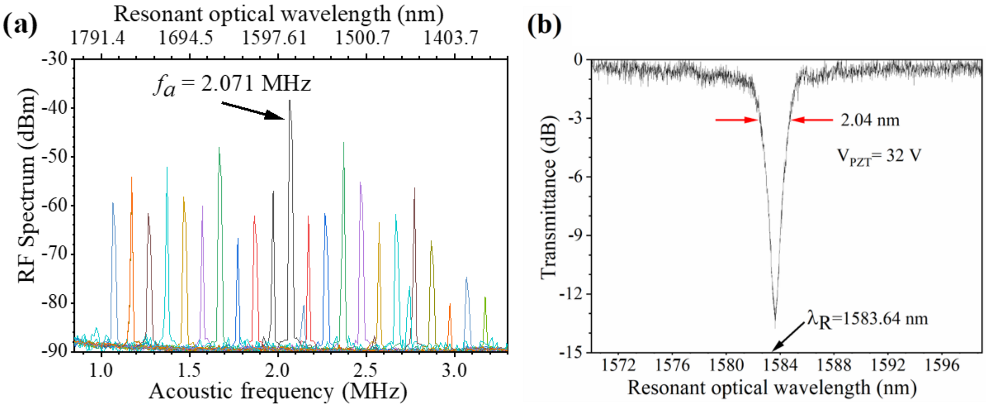

Figure 5. (a) Measured RF spectra to expose the non-flat frequency response of the PZT disk in a range of acoustic frequencies between 1.06 MHz and 3.17 MHz. The best performance of the PZT disk corresponds to the highest peak located at 2.071 MHz. (b) AO resonance produced by a TFAW at the acoustic frequency (f_a) of 2.071 MHz with V_{PZT} equal to 32 V.

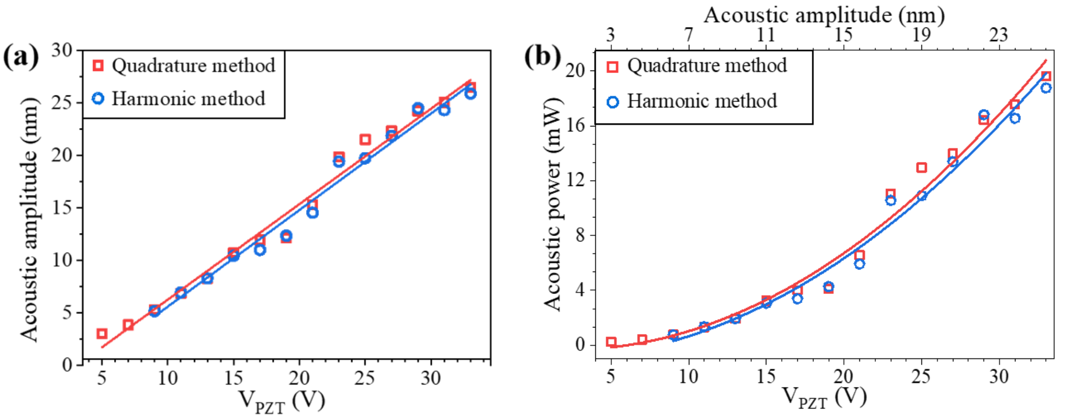

Figure 6. (a) Acoustic wave amplitude as a function of the V_{PZT} voltage. (b) Acoustic power as a function of the V_{PZT} and the acoustic amplitude. The solid lines in both figures indicate the measurements based on the quadrature condition method (red line) and the method based on the difference between the first harmonic amplitudes (blue line).

quadrature condition method below 8.3 % for all the reported measurements, from which a rate of change of 0.9 nm per V_{PZT} is measured. Additionally, an estimation of the acoustic power (P_a), which is a function of the acoustic amplitude and the fiber parameters, can be calculated from the following equation [51]

$$P_a = 4\rho u_0^2(\pi^7 C_{ext} R^5 f_a^5)^{1/2}, \tag{8}$$

where ρ represents the density of the material, 2200 kg m^{-3} for silica, C_{ext} is the extensional velocity of the acoustic waves propagating along the fiber, with a value of 5760 m s^{-1} for silica, R is the radius of the optical fiber (62.5 µm) and f_a stands for the acoustic wave frequency. Figure 6(b) depicts the acoustic power as a function of the applied voltage and the corresponding acoustic amplitude measured with each method. The maximum and the minimum acoustic measured powers were 19.63 mW and 256.9 µW, when applying a V_{PZT} of 33 V and 5 V, respectively.

From these results, both methods yield similar results when exceeding 10 nanometers in amplitude, but the minimum detection limit is obtained under the quadrature condition method, from which a direct measurement of the acoustic wave amplitude is achieved by determining the V_{MAX} and V_{SIGNAL} values. In contrast, the method based on the measured amplitudes of the harmonic frequencies, exhibits an inferior detection limit (4.1 nm) and requires additional numeric calculations. In the next sections the quadrature condition method is used to determine the amplitude of the acoustic wave.

3.2 Attenuation coefficient

The attenuation coefficient of the acoustic wave is evaluated by measuring the acoustic wave amplitude within a total interaction length of 1 m, considering measurements at different positions in steps of 10 cm in length. As a first example, the acoustic frequency (f_a) and the V_{PZT} are fixed at 2.1 MHz and 30 V, respectively. Figure 7(a) illustrates these measurements and exposes the decay in amplitude of the acoustic wave with an exponential decay function in the form $u = u_0 e^{-\alpha z}$, where u_0 denotes the initial amplitude measured at the point where the fiber is glued to the horn, z is the distance at which the measurement is obtained, and α represents the attenuation coefficient. This evaluation of the acoustic wave amplitude reveals an attenuation coefficient of 0.435 m^{-1} for the acoustic frequency of 2.1 MHz. Besides this result, the acoustic coefficient is also measured at the operation limits of the PZT, at around 1 MHz and 3 MHz, respectively, as shown in Figure 7(b). As it can be observed, the largest amplitude is generated at 2.1 MHz, since the PZT is optimized to operate in the 2-MHz region. From Figure 7(c), the relation between the attenuation coefficient and the acoustic frequency is presented in more details for the range of frequencies between 1 MHz and around 3 MHz. The variation of the attenuation coefficient is exposed as a linear decay function, from which a rate of change of –0.085 m^{-1} per MHz is estimated.

3.3 Group velocity and group attenuation for an acoustic wave packet

For the analysis of the group velocity and the group attenuation coefficient, an acoustic wave packet is generated by driving the PZT disk with a burst signal composed of an integer number of the acoustic wave periods, the effective length (L_{eff}) of this packet must be shorter than the interaction length. The packet propagates along the optical fiber, in a scheme consisting of around 1-m long AO interaction length. In such a way, the propagation of the acoustic wave packet is analyzed by recording the transmitted light at the resonant

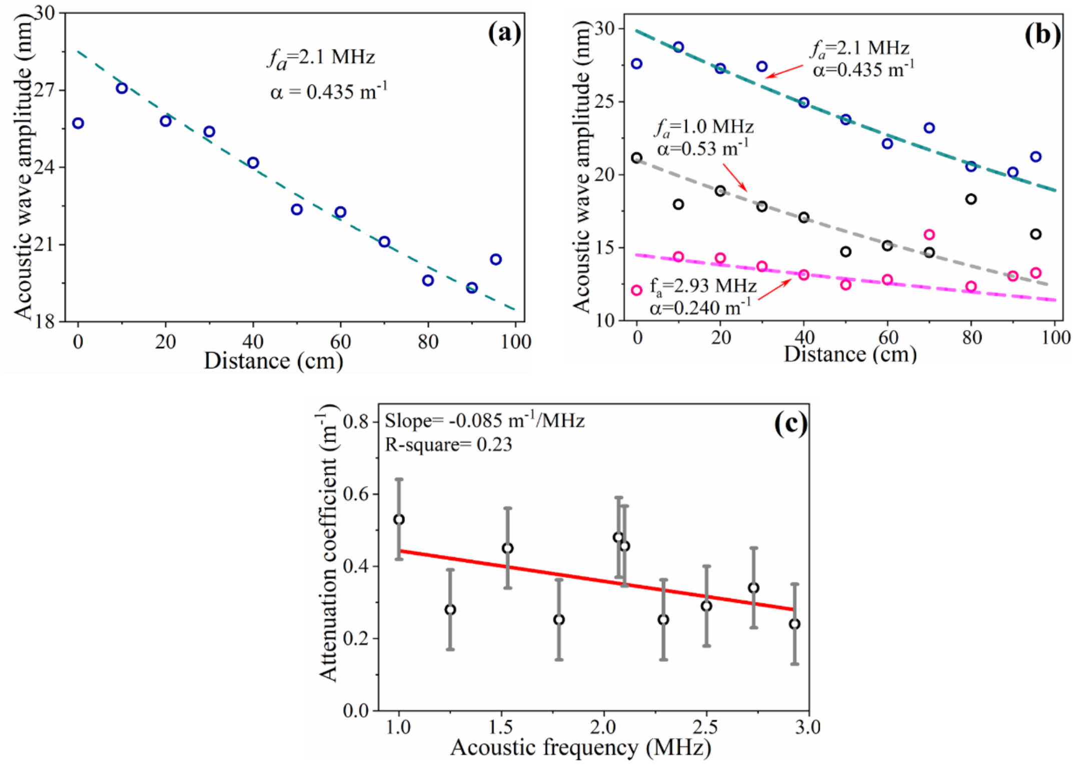

Figure 7. (a) Determination of the attenuation coefficient at 2.1 MHz of acoustic frequency. (b) Measurement of the attenuation coefficient at the operation limits of the PZT, including the acoustic frequencies of 1 MHz, 2.1 MHz and 2.93 MHz. (c) Linear approximation for the rate of change of the attenuation coefficient in a range of frequencies from 1 MHz to 2.93 MHz. In all measurements, V_{PZT} is maintained fixed at 30 V.

optical wavelength (λ_R) [14]. Thus, for a given acoustic frequency, there exists a resonant wavelength at which the intermodal coupling is best satisfied, see Figure 5(b). Therefore, the propagation of the acoustic wave packet is analyzed by measuring the transmission of the input light power at the resonant optical wavelength, so the transmitted light is affected when the acoustic wave packet travels along the AO interaction length. Figure 8(a) illustrates the transmittance at the optical resonant wavelength of 1533.62 nm, when a traveling acoustic wave packet of 2.6154 MHz - generated with a burst of 210 cycles and V_{PZT} of 38 V- is launched into the uncoated optical fiber. The time interval that is required to switch from the level of maximum to minimum transmittance is measured as 85.5 µs. This is the required time for the acoustic wave packet to be totally inserted at the beginning of the AO interaction length. The opposite behavior is observed around 342.5 µs later, when the acoustic packet leaves the AO interaction length, producing a 91.1 µs rise time. One also observes a smooth recovery of the transmittance along the fiber, after it reaches the minimum of transmittance, over the 85.5 µs - 342.5 µs time interval. This effect is essentially due to the attenuation of the acoustic wave packet from which a group attenuation coefficient (α_g) is associated to the wave packet. For the given AO interaction length of 97.8 cm, and the time that the acoustic packet takes to travel across it (342.5 µs), the group velocity (v_g) is measured as 2873.7 m s^{-1}. For this calculation, an effective length (L_{eff}) for the wave packet (the physical distance of the packet along the fiber) is estimated as 0.25 m. Using these parameters, the transmission of light can be expressed by the following equation [14]

$$T_R = 1 - \sin^2(C_0 e^{-\alpha_g v_g t} L_{eff}), \quad (9)$$

where C_0 is the coupling coefficient at a distance $z = 0$, α_g the group attenuation coefficient and t the time. The estimated value for α_g is 0.48 m^{-1} at f_a = 2.6154 MHz, as shown in the red dotted line in Figure 8(a).

With the objective of analyzing the group attenuation coefficients for different acoustic wave packets, the transmittance is analyzed at the acoustic frequencies of 2.4466 MHz and 2.6935 MHz, having a corresponding resonant optical wavelength of 1564.55 nm and 1520.67 nm, respectively, which are located near the ends of the operating tuning range of the TLD. These traces along with their respective fitting attenuation curve (dotted lines) are depicted

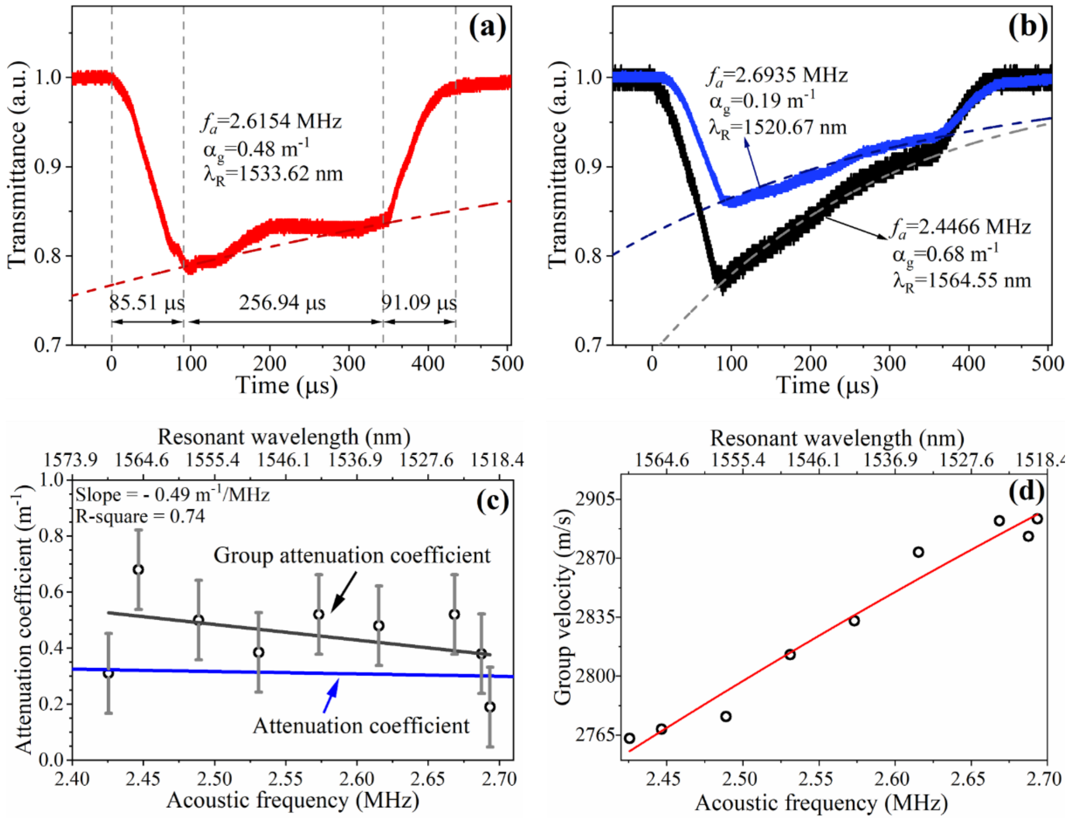

Figure 8. Transmittance of light at the resonant optical wavelength due the propagation of an acoustic wave packet with acoustic frequency of (a) 2.6154 MHz (b) 2.4466 MHz and 2.6935 MHz, with V_{PZT} at 38 V, 13.7 V and 41.7 V, respectively. The dashed lines in (a) and (b) indicate the fitting of transmission as a function of time. (c) Group attenuation coefficient (gray line) as a function of acoustic frequency, and attenuation coefficient (blue line) as it was measured for harmonic waves (see Figure 7(c)). (d) Measurement of group velocity as a function of the acoustic frequency. The acoustic frequency is varied in a range between 2.4255 MHz and 2.6935 MHz, with corresponding resonant optical wavelengths of 1569.39 nm and 1520.67 nm, respectively.

in Figure. 8(b), where group attenuation coefficients with values of 0.68 m^{-1} and 0.19 m^{-1} were measured at 2.4466 MHz and 2.6935 MHz, respectively. A more detailed measurement of the group attenuation coefficient is shown in Figure 8(c) with black dots, the variation of α_g is approximated to a linear decay function (gray line), from which a rate of change of –0.48829 m^{-1} per MHz is estimated. In this same figure, the linear fitting of the attenuation coefficient reported in Figure 7(c) is also presented (blue line) for the same range of frequencies for comparison. This last result suggests a higher attenuation for the acoustic wave packed in the 2-MHz region, because of the dispersion effects, which agrees with the results reported in [14] and [31], where values for the attenuation coefficients are reported considering an acoustic wave packet and a continuously TFAW, respectively. Figure 8(d) illustrates the measured group velocities as a function of the acoustic frequency. The frequency is varied in a range between 2.4255 MHz and 2.6935 MHz. As it can be observed, the group velocity increments according to the increment of the acoustic frequency, exposing a cuasi linear rate change of 520 m s^{-1} per MHz.

3.4 Acoustic wavelength and dispersion relation

A characterization of the acoustic wavelength and its dispersion relation is performed by implementing a standing flexural acoustic wave along the AO interaction length. For this purpose, at the opposite end to the aluminum concentrator horn, see Figure 4, the fiber is immersed in a drop of tin welding to induce acoustic reflection which gives rise to the formation of a standing flexural acoustic wave. To verify the acoustic reflection effect at the attached point, an acoustic

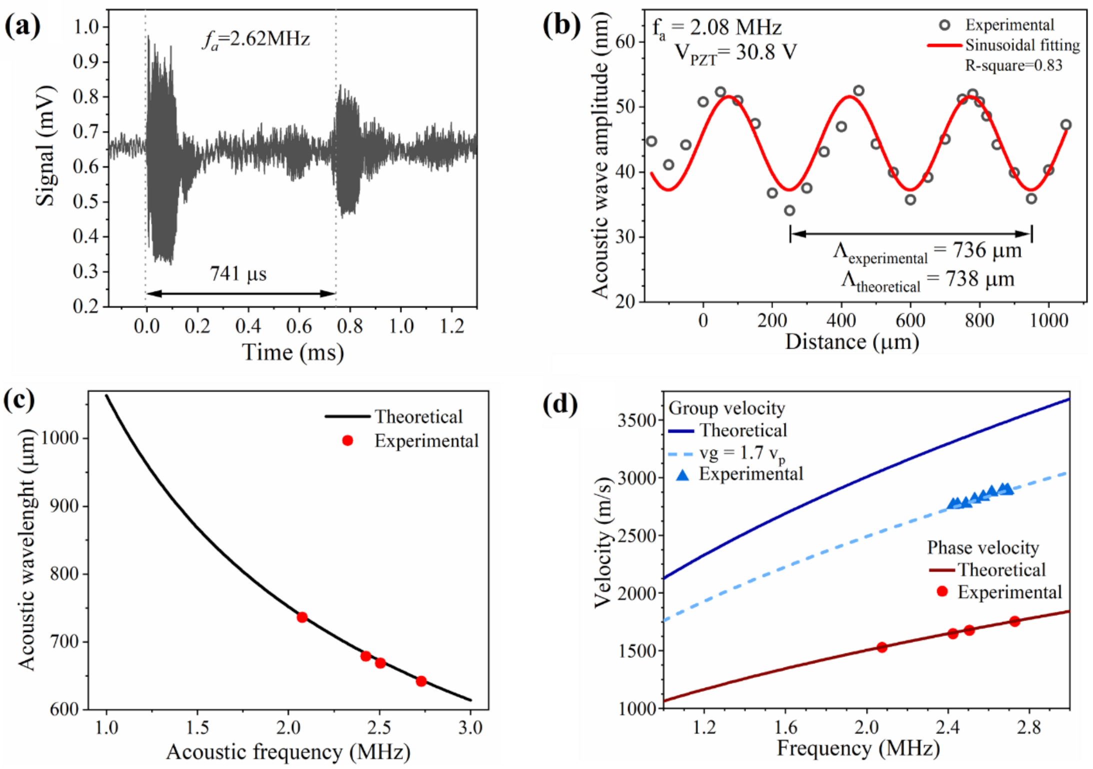

Figure 9. (a) Estimation of the acoustic reflection for an optical fiber immersed in a drop of tin welding. (b) Amplitude of the standing flexural acoustic wave as a function of AO interaction length. (c) Acoustic wavelength for acoustic frequencies in a range between 2.08 MHz and 2.73 MHz. (d) Phase and group velocity as a function of the acoustic frequency. The solid lines indicate theoretical curves and fittings.

packet composed of 220 periods of 2.6154 MHz in frequency is first measured at the beginning of its propagation, and then measured after its reflection. Figure 9(a) verifies the acoustic reflection of the wave packet after traveling an AO interaction length of 1 m. Figure 9(b) shows the measured acoustic wave amplitude along a few cycles of the generated standing flexural acoustic wave. For this measurement, the AO interaction length is reduced to 4 cm. A TFAW with an acoustic frequency of 2.07538 MHz is introduced maintaining fixed the V_{PZT} at 30.8 V, and the acoustic amplitude of the resulting standing wave was measured in steps of 50 μm along a total measurement length of 1.2 mm. The red line in Figure 9(b) illustrates a sinusoidal fitting of the experimental measurements, the acoustic wavelength is measured from the 2-fold period of the standing wave, resulting in a 736 μm acoustic wavelength. Figure 9(c) depicts a few measurements of the acoustic wavelength for the range of acoustic frequencies at which the PZT disk performs its optimal performance, between 2 MHZ and 2.7 MHz. In addition, a theoretical estimation of the acoustic wavelength (Λ) is included in the solid black line, which is obtained from the following equation [51]

$$\Lambda = \sqrt{\frac{\pi R C_{ext}}{f_a}}, \tag{10}$$

considering C_{ext} = 5760 m s^{-1}, R = 62.5 μm and the acoustic frequency ranging from 1 MHz to 3 MHz. The phase velocity (v_p) is calculated from the product of the acoustic wavelength and the acoustic frequency, as presented in Figure 9(d). In this same figure, and with the purpose of comparing the connection within the results obtained in the previous subsection, the group velocity (v_g) is included in the graphic. The results show reasonably good agreement with the relation between the phase and group velocities for an acoustic wave in a cylindrical rod [52], from which a factor of two es expected between phase and group velocities (v_g = 2v_p). However, the experimental results reveal a factor 1.7 higher for the group velocity.

4. Conclusions

An experimental study of traveling flexural acoustic waves along a standard optical fiber is reported. Initial experiments were focused on analyzing the FTI sensor that has been used for the characterization under two different measurement methods for the detection of nanometric displacements. One method relies on amplitude measurements satisfying the quadrature condition, from which a detection limit from 0.5 nm is demonstrated, while the maximum value preserving a linear response is 30.1 nm. The alternative method, whose operation depends on the harmonics of the interference signal, demonstrates a minimum detection limit of 4.1 nm. Thus, both of the reported methods validate their potential use to detect nanometric displacements associated to traveling flexural acoustic waves along an optical fiber. Following this objective, the acoustic wave parameters, such as amplitude, attenuation coefficient, wavelength and velocity were measured. The obtained results allow to estimate an attenuation coefficient for the flexural acoustic wave ranging from 0.53 m^{-1} to 0.24 m^{-1}, corresponding to acoustic frequencies in a span interval from 1 MHz to 2.93 MHz, respectively. Additionally, by propagating a burst packet of acoustic waves, the group attenuation coefficient and the group velocity were determined. Besides, by intentionally inducing a standing flexural acoustic wavelength, a measurement of the acoustic wavelength and the phase velocity were obtained. The comparison between group and phase velocities reveals that group velocity is larger by a factor of 1.7. The obtained results demonstrate the application of the FTI to perform a detailed characterization of in-fiber AO optic devices based on flexural acoustic waves.

Declaration of Competing Interest

The authors declare that they have no known competing financial interests or personal relationships that could have appeared to influence the work reported in this paper.

Funding

This work was supported by Consejo Nacional de Humanidades, Ciencia y Tecnología (CONAHCyT) "Ciencia de Frontera 2019" under Grant 217560, and in part by grant: TED2021-130200B-I00 co-funded by the Ministerio de Ciencia e Innovación of Spain (MCIN/ AEI/10.13039/ 501100011033/) and the European Union NextGenerationEU/PRTR.

Acknowledgments

E. Hernández-Escobar thanks CONAHCyT postdoctoral fellow 3787819, Y. Navarro-Martínez was supported by CONAHCyT doctoral grant 837841, M. V. Hernández-Arriaga thanks CONAHCyT postdoctoral fellow 2269202

References

[1] Kim Y and Neikirk D P 1995 Micromachined Fabry-Perot cavity pressure transducer. *IEEE Photonics Technology Letters* **7**(12) 1471-1473.

[2] Wang A, Xiao H, Wang J, Wang Z, Zhao W and May R G 2001 Self-calibrated interferometric-intensity-based optical fiber sensors. *Journal of lightwave technology* **19**(10) 1495.

[3] Wang X, Xu J, Zhu Y, Cooper K L and Wang A 2006 All-fused-silica miniature optical fiber tip pressure sensor. *Optics letters* **31**(7) 885-887.

[4] Choi H Y, Park K S, Park S J, Paek U C, Lee B H and Choi E S 2008 Miniature fiber-optic high temperature sensor based on a hybrid structured Fabry–Perot interferometer. *Optics letters*, **33**(21) 2455-2457.

[5] Lee C E and Taylor H F 1991 Fiber-optic Fabry-Perot temperature sensor using a low-coherence light source. *Journal of lightwave technology*, **9**(1) 129-134.

[6] Starodumov A N, Zenteno L A, Monzon D and De La Rosa E 1997 Fiber Sagnac interferometer temperature sensor. *Applied Physics Letters* **70**(1) 19-21.

[7] Zhu J J, Zhang A P, Xia T H, He S and Xue W 2010 Fiber-optic high-temperature sensor based on thin-core fiber modal interferometer. *IEEE Sensors Journal* **10**(9) 1415-1418.

[8] Villatoro J, Finazzi V, Minkovich V P, Pruneri V and Badenes G 2007 Temperature-insensitive photonic crystal fiber interferometer for absolute strain sensing. *Applied Physics Letters* **91**(9) 091109.

[9] Kanellopoulos S E, Handerek V A and Rogers A J 1995 Simultaneous strain and temperature sensing with photogenerated in-fiber gratings. *Optics Letters* **20**(3) 333-335.

[10] Du Y, Chen Y, Zhuang Y, Zhu C, Tang F and Huang J 2017 Probing nanostrain via a mechanically designed optical fiber interferometer. *IEEE Photonics Technology Letters* **29**(16) 1348-1351.

[11] Shaimerdenova M, Ayupova T, Sypabekova M and Tosi D 2020 Fiber optic refractive index sensors based on a ball resonator and optical backscatter interrogation. *Sensors* **20**(21) 6199.

[12] Kim D W, Shen F, Chen X and Wang A 2005 Simultaneous measurement of refractive index and temperature based on a reflection-mode long-period grating and an intrinsic Fabry–Perot interferometer sensor. *Optics letters* **30**(22) 3000-3002.

[13] Aydin D, Barnes J A and Loock H P 2023 In-fiber interferometry sensors for refractive index. *Applied Physics Reviews* **10**(1).

[14] Alcusa-Sáez E P, Díez A, González-Herráez M and Andrés M V 2014 Time-resolved acousto-optic interaction in single-mode optical fibers: characterization of axial nonuniformities at the nanometer scale. *Optics Letters* **39**(6) 1437-1440.

[15] Pohl A A, Oliveira R A, Da Silva R E, Marques C A, Neves P D T, Cook K, Canning J and Nogueira R N 2013 Advances and new applications using the acousto-optic effect in optical fibers. *Photonic Sensors* **3** 1-25.

[16] Qian H, Shao L Y, Zhang W, Zhang X, He H, Luo B, Pan W, Zou X and Yan L 2018 Fiber-optic viscometer with all-fiber acousto-optic superlattice modulated structure. *Journal of Lightwave Technology* **36**(18) 4123-4128.

[17] Wang T, Zheng S and Yang Z 1998 A high precision displacement sensor using a low-finesse fiber-optic Fabry-

Pérot interferometer. *Sensors and Actuators A: Physical* **69**(2) 134-138.
[18] Cheng L K, Hagen R A, Schriek L N, Toet P M and Togt O V 2017 Fiber interferometer combining sub-nm displacement resolution with miniaturized sensor head. *25th Optical Fiber Sensors Conference (OFS)* IEEE.
[19] Lu Y, Xiel F and Wu S 2008 On-line displacement measurement using a high stability multiplexed optical fiber interferometer system. *2nd IEEE International Nanoelectronics Conference* IEEE.
[20] Dash J N, Jha R, Villatoro J and Dass S 2015 Nano-displacement sensor based on photonic crystal fiber modal interferometer. *Optics letters* **40**(4) 467-470.
[21] Chen J, Zhou J and Yuan X 2014 M–Z interferometer constructed by two S-bend fibers for displacement and force measurements. *IEEE photonics technology letters* **26**(8) 837-840.
[22] Andrés M V, Foulds K W H and Tudor M J 1986 Optical activation of a silicon vibrating sensor. *Electronics Letters* **22**(21) 1097-1099.
[23] Silva R E and Pohl A A 2012 Characterization of flexural acoustic waves in optical fibers using an extrinsic Fabry–Perot interferometer. *Measurement Science and Technology* **23**(5) 055206.
[24] Andrés M V, Tudor M J and Foulds K W H 1987 Analysis of an interferometric optical fibre detection technique applied to silicon vibrating sensors. *Electronics Letters* **15**(23) 774-775.
[25] Östling D and Engan H E 1995 Narrow-band acousto-optic tunable filtering in a two-mode fiber. *Optics letters* **20**(11) 1247-1249.
[26] Lu J et al. 2018 Dynamic mode-switchable optical vortex beams using acousto-optic mode converter. *Optics letters* **43**(23) 5841-5844.
[27] Zhao J and Liu X 2006 Fiber acousto-optic mode coupling between the higher-order modes with adjacent azimuthal numbers. *Optics letters* **31**(11) 1609-1611.
[28] Culverhouse D O, Yun S H, Richardson D J, Birks T A, Farwell S G and Russell P S J 1997 Low-loss all-fiber acousto-optic tunable filter. *Optics letters* **22**(2) 96-98.
[29] Huang L, Zhang W, Li Y, Han H, Li X, Chang P, Gao F, Zhang G, Gao L and Zhu, T 2018. Acousto-optic tunable bandpass filter based on acoustic-flexural-wave-induced fiber birefringence. *Optics Letters* **43**(21) 5431-5434.
[30] Satorius D A, Dimmick T E and Burdge G L 2002 Double-pass acoustooptic tunable bandpass filter with zero frequency shift and reduced polarization sensitivity. *IEEE Photonics Technology Letters* **14**(9) 1324-1326.
[31] Ramirez-Melendez G, Bello-Jiménez M, Pottiez O and Andrés M V 2017 Improved all-fiber acousto-optic tunable bandpass filter. *IEEE Photonics Technology Letters* **29**(12) 1015-1018.
[32] Escobar E H, Jiménez M B, Avilés A C, Estopier R L, Pottiez O, Sánchez M D, Escamilla I and Andrés M V 2019 Experimental study of an in-fiber acousto-optic tunable bandpass filter for single-and dual-wavelength operation in a thulium-doped fiber laser. *Optics express* **27**(26) 38602-38613.
[33] Cuadrado-Laborde C, Bello-Jiménez M, Díez A, Cruz J L and Andrés M V 2014 Long-cavity all-fiber ring laser actively mode locked with an in-fiber bandpass acousto-optic modulator. *Optics Letters* **39**(1) 68-71.
[34] Yue W, Chen T, Kong W, Ji Z, Yin L, Huang G, He Z and Shu R 2021 Flexible wavelength generation from a Yb-doped fiber laser incorporating multifunctional acousto-optic tunable filter. *Optics Letters* **46**(5) 1041-1044.
[35] Bello-Jiménez M, Hernández-Escobar E, Camarillo-Avilés A, Pottiez O, Díez A and Andrés M V 2018 Actively mode-locked all-fiber laser by 5 MHz transmittance modulation of an acousto-optic tunable bandpass filter. *Laser Physics Letters* **15**(8) 085113.
[36] Alcusa-Sáez E, Díez A and Andrés M V 2016 Accurate mode characterization of two-mode optical fibers by in-fiber acousto-optics. *Optics Express* **24**(5) 4899-4905.
[37] Rivera-Pérez E, Carrascosa A, Díez A, Alcusa-Sáez E P, Andrés M V 2018 An approach to the measurement of the nonlinear refractive index of very short lengths of optical fibers. *Applied Physics Letters* **113**(1) 011108.
[38] Kim B Y, Blake J N, Engan H E and Shaw H J 1986 All-fiber acousto-optic frequency shifter. *Optics Letters* **11**(6) 389-391.
[39] Birks T A, Russell P S J and Culverhouse D O 1996 The acousto-optic effect in single-mode fiber tapers and couplers. *Journal of lightwave technology* **14**(11) 2519-2529.
[40] Brientin A, Leduc D, Gaillard V, Girard M and Lupi C 2021 Numerical and experimental study of a multimode optical fiber sensor based on Fresnel reflection at the fiber tip for refractive index measurement. *Optics & laser technology*, **143** 107315.
[41] Murphy K A, Gunther M F, Vengsarkar A M and Claus R O 1991 Quadrature phase-shifted, extrinsic Fabry–Perot optical fiber sensors. *Optics letters* **16**(4) 273-275.
[42] Pullteap S 2012 Development of an optical fiber based interferometer for small vibration measurements. *11th International Conference on Optical Communications and Networks (ICOCN)*IEEE.
[43] Pullteap S and Seat H C 2015 An extrinsic fiber Fabry-Perot interferometer for dynamic displacement measurement. *Photonic Sensors* **5** 50-59.
[44] Zhang Z, Jiang C, Wang F, Huang Z, Shen L and Li C 2020 Quadrature phase detection based on an extrinsic Fabry–Pérot interferometer for vibration measurement. *Optics Express* **28**(22), 32572-32583.
[45] Sudarshanam V S and Srinivasan K 1989 Linear readout of dynamic phase change in a fiber-optic homodyne interferometer. *Optics Letters* **14**(2) 140-142.
[46] Deferrari H A and Andrews F A 1966 Laser Interferometric Technique for Measuring Small-Order Vibration Displacements. *The journal of the Acoustical Society of America* ***39***(5A) 979-980.
[47] Ohtsuka Y 1982 Dynamic measurements of small displacements by laser interferometry. *Transactions of the Institute of Measurement and Control* **4**(3) 115-124.
[48] Sudarshanam V S 1992 Minimum detectable phase shift in spectrum-analysis techniques of optical interferometric vibration detection. *Applied optics* **31**(28) 5997-6002.
[49] Arfken G B and Weber H J 2005 Bessel Functions in *Mathematical methods for physicists* 6th edition (New York: Elsevier Academic Press) p 679.
[50] Russell P S J and Liu W F 2000 Acousto-optic superlattice modulation in fiber Bragg gratings. *JOSA A* **17**(8) 1421-1429.

[51] Blake J N, Kim B Y, Engan H E and Shaw H J 1987 Analysis of intermodal coupling in a two-mode fiber with periodic microbends. *Optics letters* **12**(4) 281-283.

[52] Humar J 2012 *Dynamics of structures*. (Ottawa: CRC press.)